Effect of fabrication conditions on the porous structure of polyacrylonitrile-derived carbons and their influence on dye adsorption and gas separation

Surfaces and Interfaces 73 (2025) 107571

Contents lists available at ScienceDirect

Surfaces and Interfaces

journal homepage: www.sciencedirect.com/journal/surfaces-and-interfaces

Effect of fabrication conditions on the porous structure of polyacrylonitrile-derived carbons and their influence on dye adsorption and gas separation

Lidia Domínguez-Ramos [a,b,c], Diego Gómez-Díaz [a], M. Sonia Freire [a], Giulio Malucelli [d], Massimo Lazzari [b,c,*], Julia González-Álvarez [a]

[a] Departamento de Ingeniería Química, ETSE, Universidade de Santiago de Compostela, Rua Lope Gómez de Marzoa s/n, 15782 Santiago de Compostela, Spain
[b] Departamento de Química Física, Facultade de Química, Universidade de Santiago de Compostela, Avenida das Ciencias s/n, 15782 Santiago de Compostela, Spain
[c] Centro Singular de Investigación en Química Biolóxica e Materiais Moleculares (CiQUS), Universidade de Santiago de Compostela, 15782 Santiago de Compostela, Spain
[d] Department of Applied Science and Technology, Politecnico di Torino, Viale Teresa Michel 5, 15121 Alessandria, Italy

ARTICLE INFO

Keywords:
Polyacrylonitrile
Carbon
Adsorption
Carbon dioxide
Dye
Separation

ABSTRACT

The adsorption technique for pollutant separation has increased the number of applications, and one of the most interesting aspects is focused on the fabrication of new tailored materials. This research is focused on producing carbons as adsorbent materials from polyacrylonitrile (PAN), aiming to promote the presence of such heteroatoms as nitrogen and sulfur, already embedded in the precursor and added during fabrication, respectively. The use of various fabrication conditions (temperature, amount of activating agent, KOH and/or sulfur, S) has allowed the production of carbons with different pores distributions (microporous and mesoporous materials) and containing heteroatoms. In general, it was observed that both an increase in temperature and a higher amount of KOH or S tend to increase the size of the pores generated in the carbons. These materials have been used for CO_2 separation and for the removal of industrial red dye, demonstrating the significant role of the carbon's porous structure in the adsorption process. On the one hand, for CO_2 separation, the microporous materials showed outstanding behavior, achieving suitable loading and selectivity values. The red dye adsorption studies proved the existence of a size exclusion effect that hinders pollutant removal, as highly microporous carbons hardly could remove the contaminants. In contrast, this separation was enhanced by slightly increasing the average pore size (values above 2 nm).

1. Introduction

The use of adsorption-based technologies to improve separation operations has gained significant relevance in recent decades, both for their application in the separation of molecules of interest in aqueous solutions or in gas streams. In addition to the positive results achieved through the improvements in this technology, both in terms of adsorbent materials and operational modes, the cost associated with such operations has been considered a key area of interest. For example, 50 % reduction in the cost of separating certain contaminants from water can be achieved [1,2].

The use of processes involving physical adsorption has become an increasingly attractive option, especially for enabling the regeneration of the adsorbent simply and cost-effectively. Many adsorbents have been developed within this adsorption type, such as carbons, zeolites, and molecular organic frameworks [3–5]. In some cases, these materials show low adsorption capacities, particularly in large-scale processing, making it necessary to continue developing systems that enhance specific characteristics tailored to certain applications.

Among the various materials used as adsorbents, porous carbons have been considered suitable candidates for adsorption/separation operations involving different types of adsorbates. This is proved by several positive aspects that enhance the adsorption capacity of both gases and substances in aqueous solution [6,7]. These positive characteristics focus not only on the high adsorption capacity but also on the low fabrication cost, easy regeneration, high thermal stability, large

* Corresponding author.
E-mail address: massimo.lazzari@usc.es (M. Lazzari).

https://doi.org/10.1016/j.surfin.2025.107571
Received 10 June 2025; Received in revised form 30 July 2025; Accepted 29 August 2025
Available online 30 August 2025

surface area, tunable porosity, and the presence of functional groups of interest [8].

The fabrication/synthesis of these materials generally involves an activation stage, which generates an extended porosity in the material and defines the porous structure characteristics. Chemical activation allows for using different reagents, with KOH being commonly employed because it tends to provide suitable material characteristics depending on the specific objective. This is because KOH typically generates large surface areas, and the activating agent-to-carbon ratio applied can define or modify the pore size distribution of materials [9].

Focusing on the raw material used in the present study, polyacrylonitrile (PAN) is considered a widely available, relatively inexpensive carbon precursor with good characteristics regarding chemical and thermal stability [10,11].

In addition, this precursor has been considered suitable for producing N-enriched carbons, which have been highlighted by various researchers for enhancing the adsorption process of various adsorbates [12,13]. Likewise, other heteroatoms have been considered doping agents, such as sulfur. However, some difficulties have been detected in incorporating sulfur into the material [14]. Sulfur-doped carbons have significantly improved the adsorption of various molecules [15,16].

Nevertheless, the presence of heteroatoms and the characteristics of the porous structure may not have a cumulative effect on the adsorption of certain substances, but rather they might generate negative influences [17,18], highlighting the difficulty of developing suitable adsorbents. As an example, a larger N-content is not always associated with the best adsorption process efficiency. In particular, an increased N-content (especially from C–*N* = *C* and C_2NH functional groups) favors adsorbent–adsorbate interactions that induces additional enthalpic contributions [17]. Additionally, it has been proposed that the increase in N-content is correlated to decreases in the N_2-accessible micro- and mesoporosity.

The present work proposes the fabrication of carbons derived from PAN under different operating conditions involving temperature, sulfuration, and activation processes. PAN is considered an excellent precursor with high carbon yields, suitable not only for the inherent introduction of different N-containing functional groups but also O- and S-containing groups though a strict control of temperature, and controlled conditions of oxidation and sulfuration, respectively [10,11,17]. The effect of these parameters on the adsorption process of pollutants (carbon dioxide in gas phase and a commercial red dye for wood in aqueous solution) is evaluated in terms of chemical and structural carbon properties, such as functional groups, surface area, and pore sizes and adsorption performance.

2. Experimental

2.1. Chemicals

Carbons were fabricated using polyacrylonitrile, PAN (150,000 g/mol; Sigma-Aldrich, Darmstadt, Germany), sulfur (>99 %, rhombic sulfur; Merck, Darmstadt, Germany) and KOH (Fisher Scientific, Hampton, USA). HCl (37 %) and NaOH (98 %), used for point of zero charge determination and to remove the excess of KOH, were purchased from Merck. Nitrogen and carbon dioxide (99.999 %) were supplied by Nippon Gases Iberia (Madrid, Spain). Red for wood GRA-200 % ($C_{17}H_{11}F_3N_3NaO_4S+$) is an industrial acidic and anionic wood dye provided by ASERPAL S.A. company (Grupo Losán S.A., Galicia, Spain).

2.2. Carbons fabrication

In this study, carbon materials (Table 1) were fabricated through a thermal treatment in a tubular furnace (Carbolite), using PAN as the polymeric precursor. The preparation of activated carbons consists of carbonization, activation, and washing with an HCl solution. The carbonization process was carried out in two stages, namely: oxidative stabilization and subsequent pyrolysis. For oxidative stabilization, PAN powder was treated with O_2 (10 mL min^{-1}) at 553 K (2 K min^{-1}) for 1 hour, facilitating the cyclization and cross-linking of PAN. Afterward, the material was held at 553 K for 30 min under an inert atmosphere of nitrogen, and then pyrolyzed at the selected temperatures between 873 and 1123 K (5 K min^{-1}) for 30 min. Activation was performed by grinding the carbonized material and mixing it with various carbon-to-KOH mass ratios (Table 1). The mixture was then heated under N_2 (10 mL min^{-1} gas flow) to temperatures between 873 and 1123 K, at which it was maintained for 2 h. The excess KOH was removed by washing the material with 100 mL of 0.1 M HCl solution, followed by distilled water until a neutral pH was achieved. The material was then filtered under vacuum and dried at 373 K for 24 h. Sulfur-doped carbons were obtained by mixing PAN with sulfur in varying mass ratios (Table 1), heating the mixture under N_2 (10 mL min^{-1}) to 553 K, and stabilizing it at this temperature for 1 hour. The resulting material was then heated under N_2 to a temperature in the previously indicated range (between 873 and 1123 K) and held at that temperature for 30 min, followed by cooling to room temperature. Finally, all carbon materials were ground in a mortar before characterization and adsorption experiments. For each experiment, the same temperature was chosen for pyrolysis, sulfur doping, and activation.

2.3. Materials characterization

The point of zero charge (pH_{PZC}) of all fabricated carbons was determined using the method reported elsewhere [19]. Briefly,

Table 1
Experimental conditions of carbon fabrication and their elemental compositions.

Material (PAN-T-S-KOH)[a]	Temperature (K)	PAN:S ratio	C:KOH ratio	Composition (wt. %)[b]			
				C	N	O	S
PAN–873–2–0	873	1:2	1:0	65.8	1.7	17.1	15.4
PAN–1123–2–0	1123	1:2	1:0	77.3	2.8	16.4	3.5
PAN–998–4–0	998	1:4	1:0	70.9	7.1	15.7	6.2
PAN–873–0–2	873	1:0	1:2	72.8	15.4	11.8	0
PAN–1123–0–2	1123	1:0	1:2	92.6	5.9	1.5	0
PAN–873–4–2	873	1:4	1:2	75.3	13.1	10.3	1.3
PAN–1123–4–2	1123	1:4	1:2	-	-	-	-
PAN–873–2–4	873	1:2	1:4	66.3	23.6	6.2	3.9
PAN–1123–2–4	1123	1:2	1:4	85.3	10.2	2.8	1.6
PAN–998–0–4	998	1:0	1:4	91.1	8.3	0.6	0
PAN–998–4–4	998	1:4	1:4	-	-	-	-
PAN–998–2–2	998	1:2	1:2	-	-	-	-

[a] : T is the treatment temperature, S is the S to PAN ratio, and KOH is the KOH-to-carbon ratio; [b]determined by XPS.

Erlenmeyer flasks were filled with 20 mL of 0.01 M NaCl solution, and the pH value was adjusted between 2 and 11 by adding 0.01 M NaOH or HCl solutions. Once the pH stabilized, 20 mg of each adsorbent carbon material was added to each flask. The samples were then shaken for 48 h to allow equilibrium to be reached using orbital air bath shaker (VWR Cienytech). The pH_{PZC} value was determined as the point where the final pH equals the initial pH.

X-ray photoelectron spectrometry (XPS) measurements were performed with a PHI 5000 Versa Probe instrument (Physical Electronics, Chanhassen, MN, USA) equipped with an Al Kα radiation (1486.6 eV) X-ray source, using Cu and Ag as calibration standards. Survey and high resolution (HR) spectra were acquired using pass energy and step energy values of 187.85 eV and 1.0 eV, and 23.50 eV and 0.2 eV, respectively. All the measurements were conducted with a focus size, power and voltage of the X-ray beam for 100 μm, 24.7 W and 15 kV, with a 45° take off angle.

The morphological and structural features were assessed by field emission scanning electron microscopy (SEM) using a FESEM Ultra Plus (Zeiss, Jena, Germany), working at 3 kV. For a better resolution, samples were sputter coated with a 5 nm Ir layer. The images were obtained using the inlens detector, on three different areas per sample and at least three different magnifications.

The specific surface area of each PAN-based carbon was determined using the Brunauer-Emmett-Teller (BET) equation, applied to N_2 adsorption-desorption isotherms at 77 K and CO_2 adsorption at 273 K. A Micromeritics ASAP 2020 sorption analyzer was employed to carry out this type of characterization. Carbon samples were degassed at 573 K for 2 h. Total pore volume was determined based on the amount of N_2 adsorbed at a relative pressure near saturation ($P/P_0 \approx 0.99$), ensuring a representative measurement of the entire pore network. To provide a more detailed characterization of the porosity, the pore size distribution and total pore volume were further refined using the two-dimensional non-local density functional theory (2D-NLDFT) model, which simultaneously analyzed both CO_2 and N_2 adsorption data.

2.4. Gas adsorption

CO_2 and N_2 adsorption isotherms were obtained with the Micromeritics ASAP 2020 volumetric system at different temperatures (273, 298, and 323 K) and at pressures between 0 and 101.3 kPa. The samples were degassed at 573 K for 2 h under vacuum to remove moisture and impurities. An ice bath in a Dewar flask was used for experiments at 173 K, while a temperature-controlled vessel equipped with a Selecta Sensoterm sensor was employed for managing the other temperatures. The adsorption experimental data obtained for CO_2 and N_2 have been employed to estimate the corresponding selectivity value employing Ideal Adsorption Solution Theory (IAST). Adsorption experiments were carried out in triplicate. The Python module pyIAST [20] has been used for IAST loading and selectivity estimation for binary mixtures of these gases.

2.5. Dye adsorption

The dye employed in the present work is Red GRA 200 % (433.34 g mol^{-1}), an industrial acidic and anionic substance provided by ASERPAL S.A. company (Grupo Losán S.A., Galicia, Spain) focused on the preparation of wood veneers boards. Adsorption experiments were performed in triplicate in batch mode using orbital air bath shaker (VWR Cienytech) at 25 °C. The experiments were carried out at natural pH (8.02), with an initial concentration of dye of aprox. 500 mg L^{-1} and carbon dosage of 0.5 g L^{-1}, using the different activated carbons fabricated in present work. Dye concentration was determined after 48 h measuring the absorbance of the liquid phase at 506 nm by using a UV-Vis spectrophotometer (V630 Jasco). Eqs. (1) and 2 were used to calculate the adsorption capacity and efficiency of the different adsorbents. .

$$q\ (mg\ g^{-1}) = (C_0 - C)\cdot V/m \quad (1)$$

$$AE\ (\%) = (C_0 - C)\cdot 100/C_0 \quad (2)$$

where C_0 and C are the initial and the residual dye concentration, respectively (mg L^{-1}), q is the capacity of adsorption (mg g^{-1}), V is the volume of the dye dissolution (L), and m is the dry mass of adsorbent used (g).

3. Results and discussion

3.1. Adsorbents characterization

3.1.1. Point of zero charge

The pH_{PZC} corresponds to the pH level, at which the charge corresponding to the adsorbent surface is null. This means that the electrostatic interactions between positive and negative charges are the same. The adsorbent surface reaches a positive character (with the existence of H^+) when the pH is below pH_{PZC}. Fig. 1 shows the determination of this parameter for three PAN-derived carbons fabricated under different experimental conditions, corresponding to the point of intersection with the diagonal shown in the graph. It can be observed that the point of zero charge changes notably depending on the fabrication/activation conditions. This procedure has been applied to all the materials manufactured in this study, and the results are presented in Table 2.

Although it is difficult to draw conclusions about the influence of the variables studied in the carbon manufacturing process, it can be concluded that an increase in temperature tends to raise the pH_{PZC} value. Regarding the role of sulfur or KOH presence, it is challenging to draw straightforward conclusions. It has been previously concluded [21] that the character of the carbon surface may influence the adsorption phenomenon because CO_2 tends to behave as a Lewis acid and the red dye is anionic type [22].

3.1.2. Surface morphology and functionalities

The effective incorporation of different functional groups in the carbons, consisting of *N*-containing groups from acrylonitrile units, *O*-containing groups by the oxidative stabilization step, and *S*-containing groups directly from sulfur addition [23] was followed by XPS (some selected spectra are shown in Fig. 2; C—N-O-S carbon compositions are summarized in Table 1). High-resolution XPS signals of N 1 s and S 2p also revealed the presence of specific groups, such as C-$S(O)_2$—C

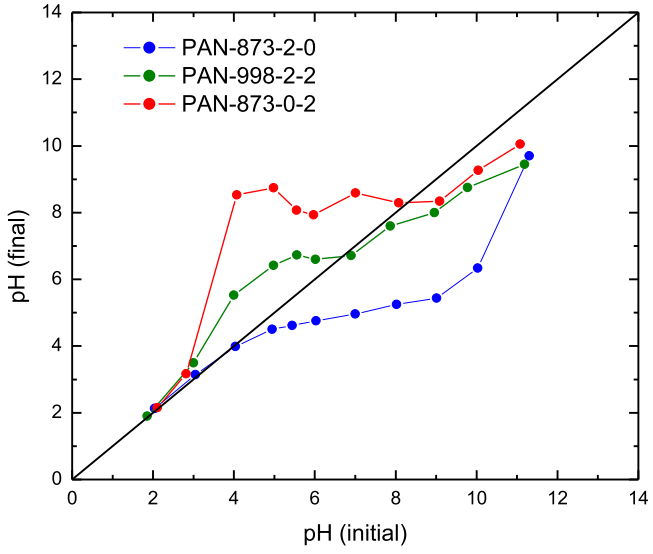

Fig. 1. Point of zero charge (pH_{PZC}) determination for different PAN-based carbons.

Table 2
Point of zero charge values for PAN-based carbons.

Material (PAN-T-S-KOH)	pH_{PZC}
PAN–873–2–0	3.8
PAN–1123–2–0	5.6
PAN–998–4–0	7.4
PAN–873–0–2	8.3
PAN–1123–0–2	7.2
PAN–873–4–2	2.5
PAN–1123–4–2	7.4
PAN–873–2–4	3.5
PAN–1123–2–4	4.4
PAN–998–0–4	7.6
PAN–998–4–4	7.4
PAN–998–2–2	6.5

sulphone and C-S-C sulfide bridges (peak centered at around 168 and 164 eV, respectively) [24], and pyridinic and pyrrolic groups (deconvoluted peak centered at around 398.4 and 400.6 eV, respectively) [25]. Concerning C groups, C—C and *C = C* bonds having peaks at around 284.5 and 286 eV are observed, being the first always the most intense in all the carbons, together with smaller peaks due to ether-like (C—O, 288 eV) and carbonyl (*C = O*, 290 eV). Functional group compositions calculated from the relative area of high-resolution element signals could be in part related to the final pyrolysis temperature, without showing significant changes with the applied S to PAN ratio and KOH-to-carbon ratio. In particular, pyridinic to pyrrolic groups ratio changes from values in the range 25/75-30/70 for the carbons fabricated at 873 K (for a direct visualization, see, e.g., Fig. 2) to a ratio in the range 55/45-50/50 for all the other carbons fabricated at 998 K or 1123 K, independently from the other components added to the precursor. The increase of pyridinic nitrogens is related to the more extended condensation of the carbon precursor at higher temperatures [23]. On the other hand, whenever sulfur is present, sulphone groups were predominant, with values of the sulphide to sulphone groups ratio showed values for all the carbons.

At the same time, the concentration of each family of functional groups, i.e., the incorporation of N, O, and S in the carbons, strongly depends on the fabrication conditions. As a general trend, the amount of *S*-containing groups appears to depend on the sulfur-to-PAN ratio and the treatment temperature, with the highest value of 15.4 wt. % for 873 K (PAN-873–2–0). Conversely, activation reduces sulfur content, with the lowest residual values for the highest KOH-to-carbon ratio and activation temperature. Nitrogen content, in the range of 0.6-17.1 wt. %, is affected by the treatment temperatures, with the lowest residual *N*-containing groups in non S-doped activated carbons activated up to 1123 K (PAN-1123–0–2). As expected, the content of *O*-containing groups decreases with activation and is inversely proportional to the treatment temperature, with the highest amount of 17.1 wt. % O for PAN-873–2–0.

From SEM analysis, it is possible to recognize some common structural morphology features that strictly depend on the activation, especially the sulfuration processes (Fig. 3). Carbonization without sulfur doping produces carbons with a compact and smooth surface, apparently without mesoporosity (Fig. 3d,e and l). Conversely, sulfur acts as a mild oxidant, stabilizing morphology and leading to vesiculated particles, approximately in the 50-200 nm range. In addition, higher activation temperatures favored the formation of bigger globular aggregates, with almost no effect of the PAN-to-sulfur and carbon-to-KOH ratio on their vesicular structures.

3.1.3. *Adsorption isotherms, porosity and surface area*

The characteristics related to the porous structure and the surface area generated in the different carbons are shown in Fig. 4(a)-(d), which plots the nitrogen adsorption and desorption isotherms at 77 K. At first glance, isotherms with different shapes are observed, which can be related to the pore structure and specifically to the pore size distribution of the fabricated materials.

First, Fig. 4a shows the behavior observed for non-activated carbons,

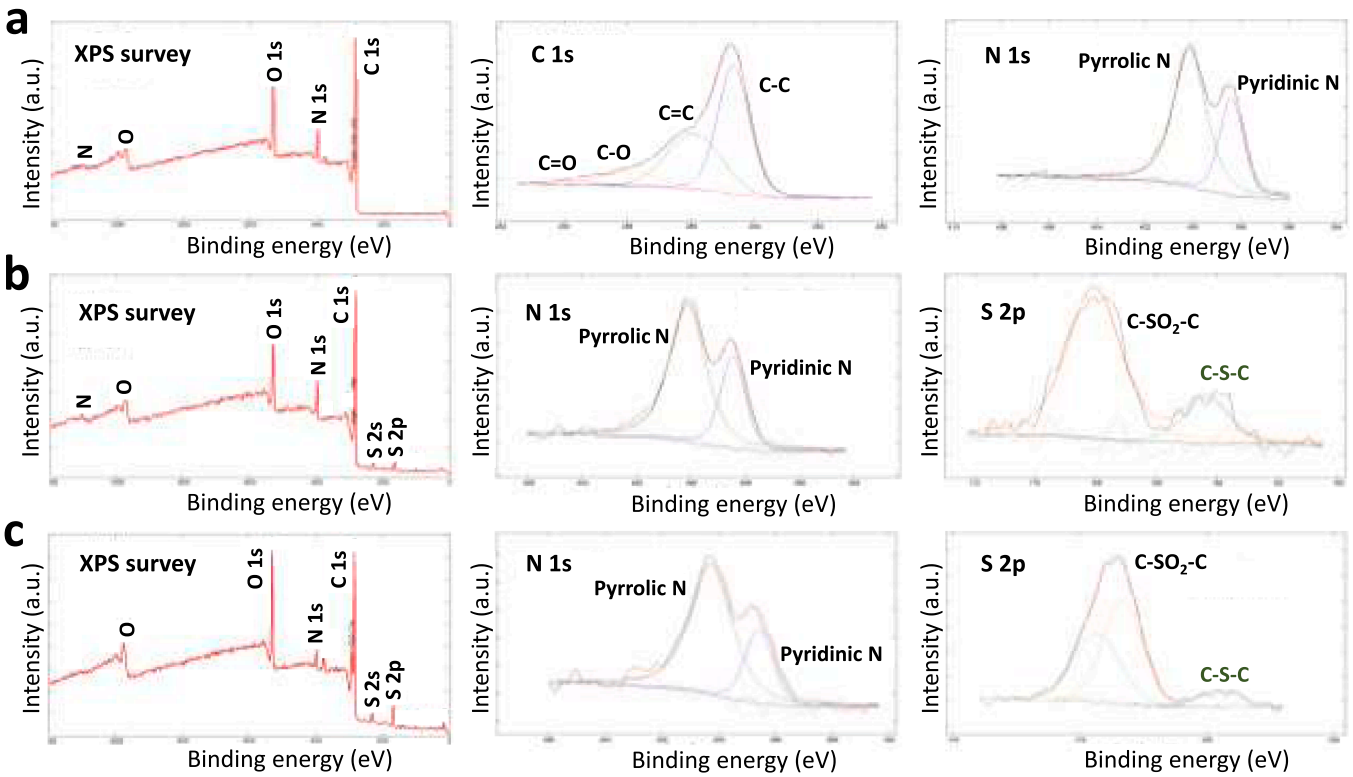

Fig. 2. Survey and high-resolution XPS spectra of PAN-873–0–2 (a), PAN-873–4–2 (b), and PAN-873–2–4 (c).

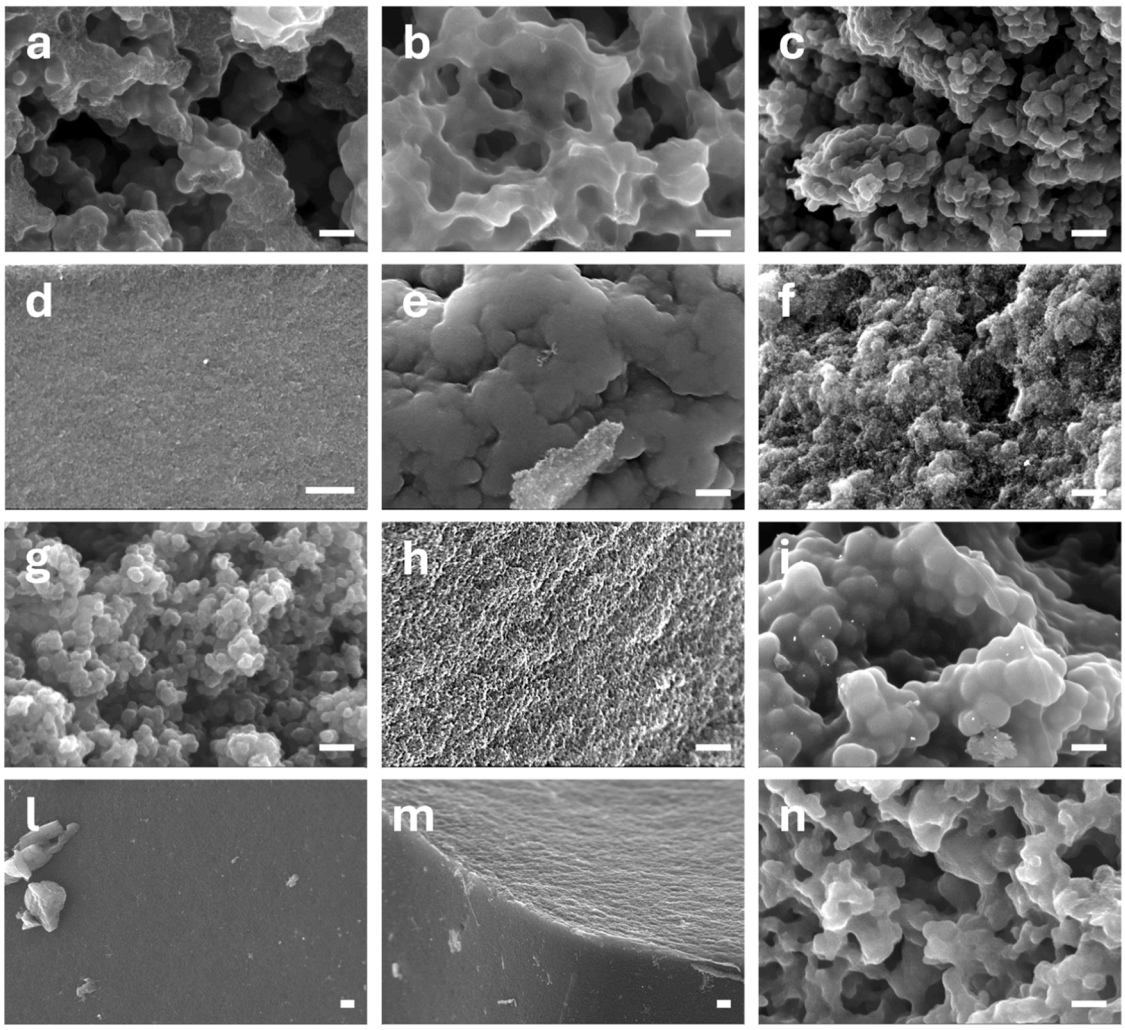

Fig. 3. Typical SEM images of carbons: a) PAN-873–2–0; b) PAN-1123–2–0; c) PAN-998–4–0; d) PAN-873–0–2; e) PAN-1123–0–2; f) PAN-873–4–2; g) PAN-1123–4–2; h) PAN-873–2–4; i) PAN-1123–2–4; l) PAN-998–0–4; m) PAN-998–4–4; n) PAN-998–2–2. Scale bar 200 nm in all the images.

carbonized at different temperatures in the presence of sulfur. It can be observed that the adsorbed amount is relatively low, and the shape of the isotherm is similar to type II, which is associated with non-porous or macroporous solids. For these carbons (PAN-873–2–0, PAN-1123–2–0, and PAN-998–4–0), the presence of a knee is observed, corresponding to the formation of the monolayer and the subsequent adsorption of multilayers. The thickness of the adsorbed multilayer generally appears to increase without limit when $P/P_0 = 1$. Moreover, it is observed that increasing the temperature used for carbon preparation, the amount of adsorbed N_2 increases significantly, indicating the generation of a larger surface area.

Fig. 4 (b-c) shows the N_2 adsorption isotherms for KOH-activated carbons, the amount adsorbed is significantly higher, especially at high relative pressures for S-doped carbons using a temperature of 1123 K (PAN-1123–2–4 and PAN-1123–4–2). This is consistent with the fact that carbon activation typically leads to an increase in the available porous structure [26] and, consequently, an increase in the specific surface area.

Among the carbons fabricated in the absence of sulfur (PAN-873–0–2, PAN-1123–0–2, and PAN-998–0–4 in plots (b) and (d)), it is worth noticing that PAN-873–0–2 and PAN-1123–0–2 show type I isotherms, and specifically of type Ib, while the PAN-998–0–4 material exhibits a quite different isotherm that agrees with type Iva [27]. Isotherm I is related in this type of materials to mainly microporous solids since it tends to form an adsorbed monolayer due to the difficulty of generating multilayers in pores with a small diameter. In the case of these materials, especially in PAN-1123–0–2, the relative pressure range in which the knee is formed is much wider, and it must be classified as type Ib isotherms. This more specific type of isotherm is related to microporous solids, but with pores included in the supramicroporous (diameters beyond 0.7 nm) type. Moreover, it is clearly observed that the range of relative pressures during the knee is much greater for PAN-1123–0–2 than for PAN-873–0–2, so an increase in temperature (keeping the amount of activating agent constant) tends to generate larger diameter pores. The isotherm of the PAN-998–0–4 material shows important differences from those previously analyzed since a continuous increase in the amount of adsorbed nitrogen is observed, and the plateau is reached at quite high relative pressures. The formation of a small hysteresis loop also appears. This type of adsorption isotherm (IVa) is usually observed for mesoporous materials. This type of solids were prepared by using a greater amount of activating agent, which is in agreement with conclusions reached in previous studies [28].

In the analysis of the role played by the presence of sulfur in the porous structure of the carbons, the comparison of the isotherms corresponding to the solids PAN-873–0–2 and PAN-873–4–2 (Fig. 4b) shows practically no differences in the shape and magnitude of the isotherms. Therefore, microporous materials are generated regardless of the presence of sulfur. On the other hand, when the material is fabricated in the same way but at higher temperature (PAN-1123–4–2), the shape of the isotherm (type IVa) changes compared to the PAN-

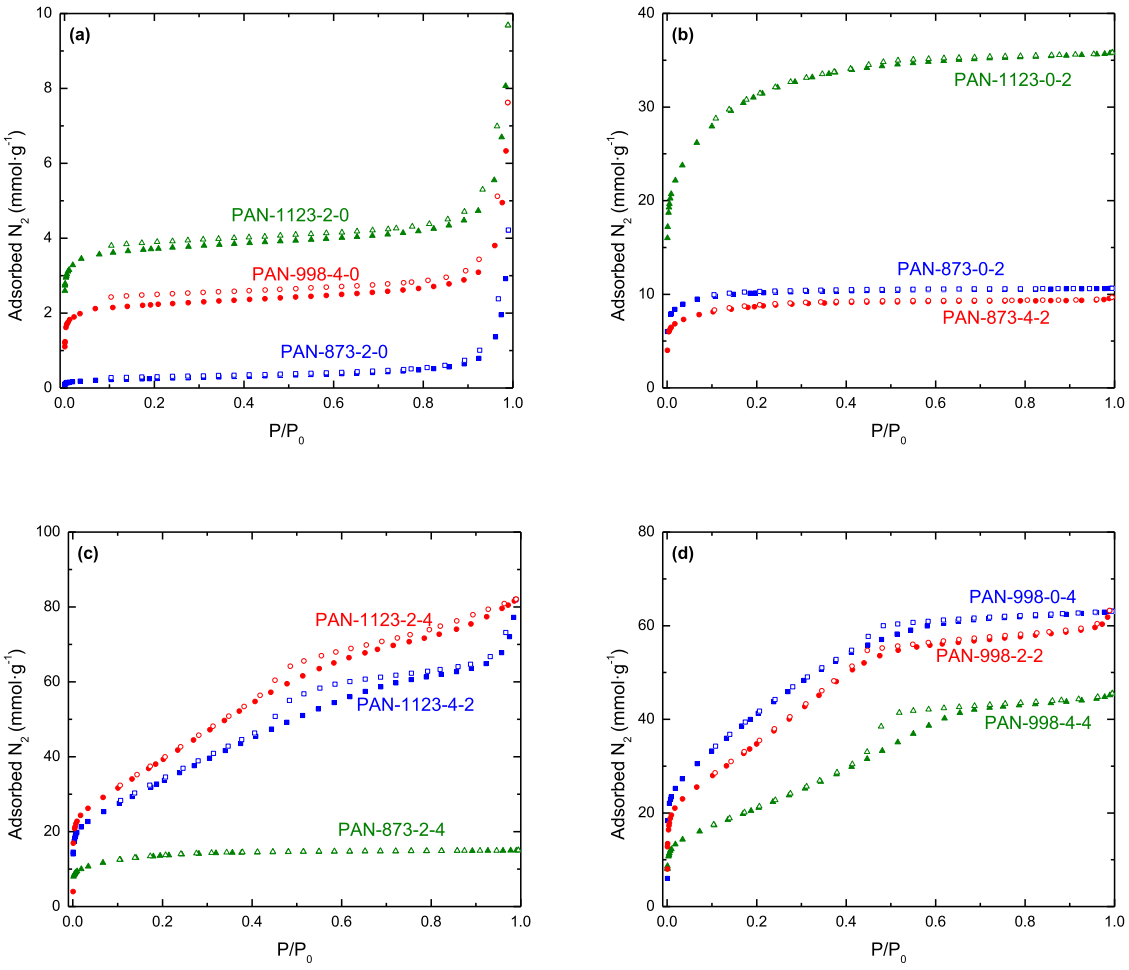

Fig. 4. Adsorption/desorption N_2 isotherms at 77 K.

1123–0–2. Therefore, an increase in temperature in the presence of sulfur significantly affects the pore size, increasing it to values characteristics of mesopores. A previous study [21] using a temperature of 1073 K and carbon-to-KOH and carbon-to-sulfur ratios of 1:4 and 1:1 (w/w), respectively, also showed a type IVa isotherm. When the effect of temperature (PAN-873–0–2 and PAN-1123–0–2) was evaluated in the absence of sulfur, a very significant increase in the adsorbed amount of nitrogen was observed (which will cause an increase in the surface area). Addionally, the shape of the adsorption isotherm did not changed, and therefore neither did the type of isotherm.

An interesting comparison involves the isotherms corresponding to PAN 873–2–4 and PAN-873–4–2 in which the amounts of KOH and sulfur were inverted, which showed the same type of microporous material with a similar magnitude in the amount adsorbed. Therefore, the amount of KOH does not seem to play an important role (in the presence of sulfur), however it seems that temperature does. This fact is confirmed by analyzing the isotherm belonging to PAN 1123–2–4 with the same conditions as PAN-873–2–4 but using a higher activation temperature. In this case, as already observed in PAN-1123–4–2, the generation of a mesoporous structure is visible, but the carbon reaches slightly higher adsorption values than PAN-1123–4–2, probably caused by the greater amount of KOH.

Based on the behaviors shown in Fig. 4, comparing the isotherms of the PAN-873–4–2 and PAN-1123–2–4 materials, and on the other hand, the PAN-873–2–4 and PAN-1123–2–4, it can be concluded that temperature plays a very important role on the size of the pores that are generated in the carbons. An increase in temperature tends to increase the presence of mesoporosity [29]. In the case of the activated carbons with a lower KOH ratio (PAN-1123–0–2 and PAN-873–0–2), an increase in temperature did not led to a change in isotherm type (caused by an increase in mesoporosity). However, they show a wider knee for high temperature, which would be related to an increase in the pore size within the microporosity [30].

Fig. 4d shows the nitrogen adsorption and desorption isotherms at 77 K for materials activated at an intermediate temperature and varying the amounts of activating agent (KOH) and sulfur (S). In all cases, the generation of activated carbons with mesoporous characteristics was observed. The comparison of the isotherms of PAN-1123–0–2 and PAN-998–0–4 materials shows that a mesoporous solid can be obtained at slightly lower temperatures if the amount of KOH increases. This behavior agrees with that observed in a previous study for PAN carbons prepared with the same experimental conditions of KOH and sulfur amounts at 1073 K [21].

Finally, PAN-998–4–4 and PAN-998–2–2 allowed to analyse the influence of the amount of KOH and S maintaining the ratio between them. It is observed that in both cases, the solids are mesoporous, but the amount of adsorbed nitrogen is significantly greater when using the smallest amounts of these chemicals. This behavior could be related to the fact that a higher amount of KOH and S can led to large pore diameter that cause a global decrease in the surface area. The nitrogen adsorption/desorption isotherms have been also used to obtain more information about the porous structure of these PAN-based carbons, specifically for the determination of the surface area using the BET equation, as well as the void volume corresponding to the micropores and mesopores. This information is included in Table 3.

As previously indicated, the surface area produced in the different

Table 3
Textural characteristics of the PAN-based fabricated materials.

Material (PAN-T-S-KOH)	S_{BET} [a] ($m^2\ g^{-1}$)	S_{BET} [b] ($m^2\ g^{-1}$)	V_{total} ($cm^3\ g^{-1}$)	V_{meso} ($cm^3\ g^{-1}$)	V_{micro} ($cm^3\ g^{-1}$)	Microporosity (%)
PAN–873–2–0	20.7	444.6	0.130	0.130	0.000	0
PAN–1123–2–0	316.8	227.5	0.279	0.223	0.056	20.1
PAN–998–4–0	191.7	181.2	0.219	0.201	0.018	8.2
PAN–873–0–2	865.1	319.8	0.368	0.032	0.336	91.3
PAN–1123–0–2	2462.4	581.3	1.240	0.328	0.912	73.5
PAN–873–4–2	692.0	297.3	0.331	0.058	0.273	82.5
PAN–1123–4–2	2723.0	496.5	2.676	2.623	0.053	2.0
PAN–873–2–4	1115.5	352.6	0.519	0.098	0.421	81.1
PAN–1123–2–4	3194.5	593.0	2.828	2.671	0.157	5.6
PAN–998–0–4	3322.0	531.9	2.184	1.651	0.533	24.4
PAN–998–4–4	1701.7	242.9	1.573	1.565	0.008	0.5
PAN–998–2–2	2837.8	428.1	2.134	1.968	0.166	7.8

[a] Determined at 77 K with N_2.
[b] Determined at 273 K with CO_2
[c]Determined at $P/P_0 = 0.99$.

materials is related to the amount of adsorbed nitrogen. However, it is limited to the relative pressure range used for BET adjustment. As previously mentioned, using an activating agent (KOH in the present study) the surface area determined using the N_2 adsorption isotherms significantly increased. For example, an increase of more than 1000 m^2/g occurred when KOH was added to PAN-873–2–0 to produce PAN-873–2–4. The same trend is observed when PAN-1123–2–0 and PAN-1123–2–4 (an increase of 2878 m^2/g) or PAN-998–4–0 and PAN-998–4–4 (an increase of 1510 m^2/g) are compared.

In general, the use of a higher temperature in the activation step accounts for generating a greater surface area when the other variables are kept constant. The same behavior is usually observed when the amount of activating agent is increased in preparing activated carbon: this finding is in agreement with previous studies [31,32]. However, analyzing the role of sulfur on this parameter, it is observed that the presence of this compound leads to a decrease in the carbon surface area, whichis of great interest for many applications of this type of material. For example, this fact is evident in the comparison of the following pairs

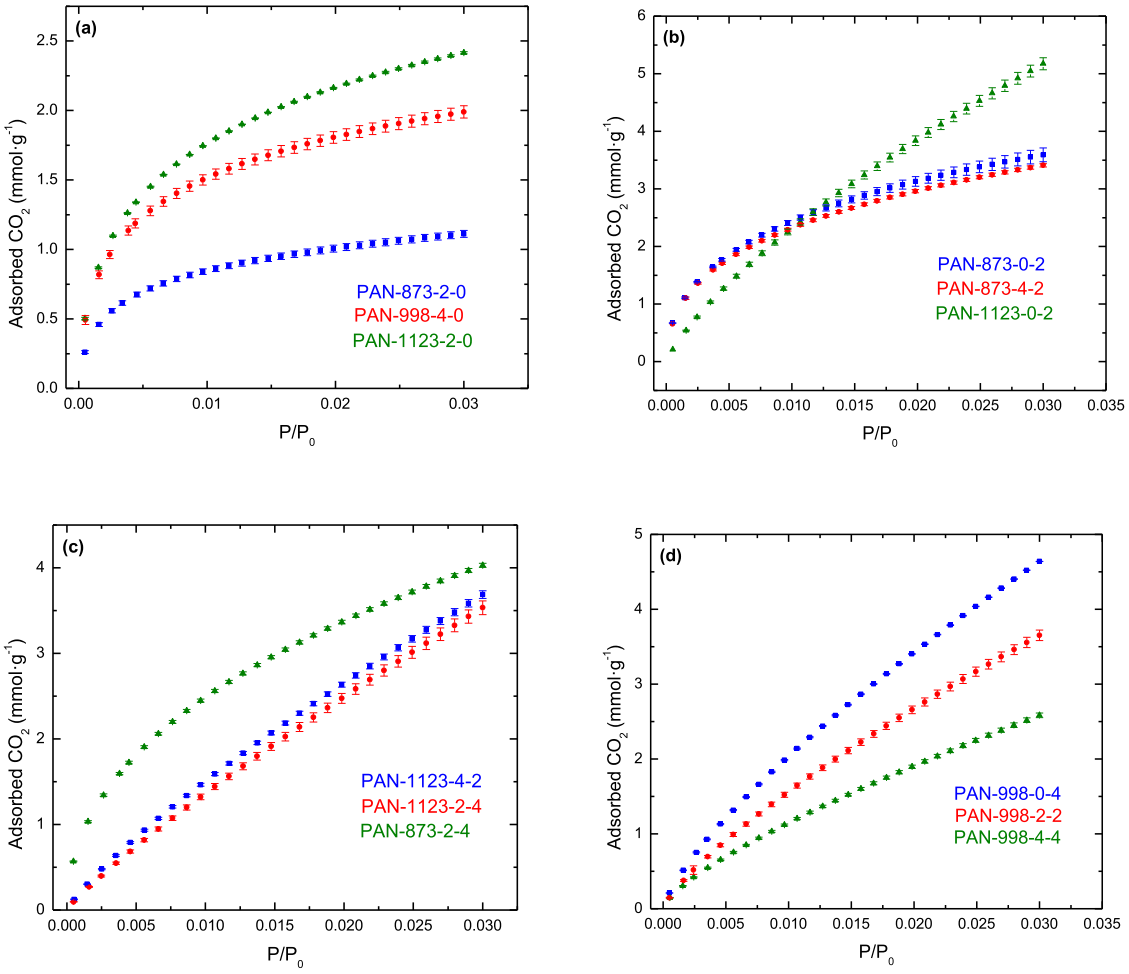

Fig. 5. CO_2 adsorption isotherms for PAN-based carbons at 273 K.

of materials PAN-873–0–2/PAN-873–4–2 (20 % lower) and PAN-873–2–4/PAN998–4–4 (51 % lower), regardless of the use of higher temperatures (PAN-1123–0–2/PAN1123–4–2), a slight increase is observed (10 % higher). In a previous work [21], it was also noticed that the presence of sulfur in activated carbons at 1073 K and with a carbon-to-KOH ratio of 1:4 (w/w) caused a decrease in the surface area (by 22 %), in agreement with the conclusions reached in present work. This behavior can be influenced by the role of sulfur, which can generate larger pores [33], as observed in Table 3.

Table 3 also shows the data corresponding to the volume generated by each pore type and, more specifically, the microporosity percentage (calculated on the basis of the pore volume). As can be seen, the conclusions drawn from the shape of the isotherms, which have been discussed, are consistent with the results obtained for the degree of microporosity determined from the volume value generated by each type of pore. Specifically, PAN-1123–4–2, PAN-998–0–4, PAN-998–0–4, PAN-998–4–4, and PAN-998–2–2 show high mesoporosity, especially notable for PAN-1123–2–4. On the contrary, PAN-873–0–2, PAN-1123–0–2, PAN-873–4–2, and PAN-873–2–4 have a highly microporous character.

These experimental results indicate that, depending on the operating conditions and the amount of activating agent and/or sulfur present in manufacturing, carbons with different porous structures can be fabricated, allowing this type of material to be used for different purposes. Then, CO_2 adsorption isotherms at 273 K have been determined to obtain more information about the porous structure of these materials.

Fig. 5 shows the different isotherms obtained for CO_2 adsorption at 273 K for the different materials. From an overall point of view, an increase in the adsorbed amount of this gas as the pressure increases is observed, although important differences appear among carbons, as in the case of those previously analyzed in Fig. 4. Similarly to the N_2 adsorption isotherms, the activation of PAN-based carbons tends to increase significantly the amount of CO_2adsorbed in some cases.

In relation to the shape of the CO_2 isotherms, those corresponding to the non-activated (PAN-1123–2–0, PAN-998–4–0, and PAN-873–2–0) and some activated materials (PAN-873–0–2, PAN-873–4–2 and PAN-873–2–4) show similar behavior, with an important enhancement of the amount of gas adsorbed at low pressures and a smoother trend when a relative pressure of 0.01 is exceeded. A different behavior was observed for the isotherms of the other materials without this change in the slope with increasing pressure, especially for activated carbons, at temperatures beyond 873 K are responsible for this change in the behavior of CO_2 adsorption isotherms, highlighting a more constant slope.

Concerning the information previously obtained and shown in Table 3, the behavior obtained for PAN-873–0–2, PAN-873–4–2, and PAN-873–2–4 is likely to be ascribed to its highly microporous character whose values of the determined degree of microporosity are higher than 80 %. PAN-1123–0–2 shows an intermediate behavior that corresponds to a slightly microporous material (73.5 %). Thus, this behavior agrees with previous conclusions about the porous characteristics of the materials since previous studies [34,35] have demonstrated that small diameter pores (microporous carbons and especially in their ultramicropores) favors CO_2 adsorption. Therefore, CO_2 has a high affinity for this type of pores at low pressures, which justifies the increased amount adsorbed in these materials at low pressures. Once the smaller pores are saturated, its lower affinity for wider pores does the adsorption decreases, and therefore the isotherm's slope with pressure is smaller. For this reason, the other activated carbons do not show the knee observed for microporous materials, and a more linear behavior is obtained. PAN-1123–0–2 does not show a very evident knee either. However, its behavior is closer to microporous materials at low pressures and mesoporous materials at high pressures.

CO_2 adsorption isotherms have also been used to determine the surface area (see Table 3) corresponding to pores within the ultramicroporosity ($D_p < 0.7$ nm) [36]. These data are inconsistent with the previous conclusions reached for non-activated carbons (PAN-1123–2–0, PAN-998–4–0, PAN-873–2–0) because the microporosity percentages are low for this type of carbons. However, considering the determined data for CO_2 adsorbed and the volume corresponding to small-sized pores, Table 3 shows that the surface area due to ultramicropores for non-activated carbons is quite large, especially when compared to the value of this parameter determined with N_2. This way, it can be concluded that the non-activated carbons have a highly ultramicroporous structure. The N_2 adsorption isotherms for these materials are not considered highly relevant, as the diffusion of such molecules in small-sized pores is very limited.

For activated carbons, it can be observed that when the surface area determined with N_2increases, the surface area determined with CO_2 (corresponding to small pores) also increases. This behavior may be due to the fact that increasing the temperature or the amount of KOH increases the availability of the porous structure, in terms of both mesopores and micropores. In any case, the increase observed in the surface area determined by N_2 adsorption is always higher than that obtained using CO_2 (Fig. 6, for instance comparing PAN-998–4–0 with PAN-998–4–4 or PAN-1123–2–0 with PAN-1123–2–4). For this reason, a decrease in the degree of microporosity is always observed in these cases.

3.2. Application of PAN-based carbons in gas separation process

Based on the PAN-based carbons characteristics previously observed under different experimental conditions, the presence of high surface areas, it allows to consider them for their application in separation processes by adsorption. One of the possible uses could be gas separation, in which the presence of micropores usually plays an important role, especially in CO_2 separation processes [37]. As previously explained, observing the adsorption isotherms shown in Fig. 5, the carbon that adsorbs amounts of CO_2 varies depending on the pressure used.

Fig. 7 shows the relationship between the amount of CO_2 adsorbed at 15 kPa and the materials' microporosity degree. The use of a pressure of 15 kPa is justified by the concentration of CO_2 in post-combustion streams, in which this gas reaches low concentrations, and therefore, it becomes more complicated the gas adsorption and separation. The experimental data obtained at this pressure allow us to observe the importance of microporosity on adsorption capacity. As the degree of microporosity increases, CO_2 adsorption also increases. This behavior agrees with the conclusions already reported in the literature [38,39] using activated carbons from different biomass precursors. It was confirmed that the adsorption of this gas in small pores enhances the adsorption [40] and also the selectivity with respect to other gases [41].

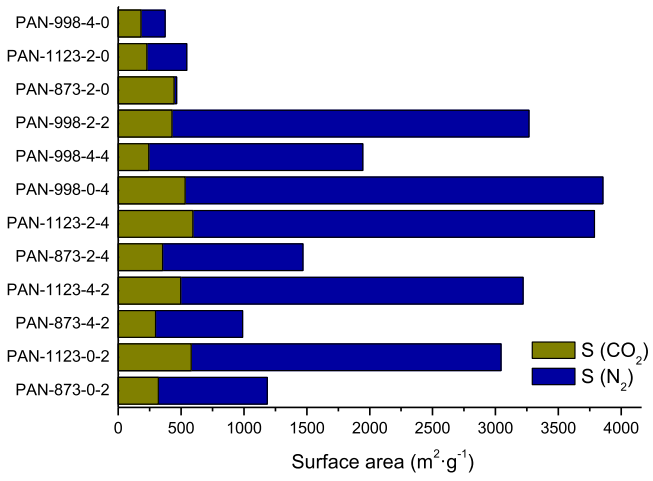

Fig. 6. Surface area determined by using adsorption isotherm data of N_2 and CO_2.

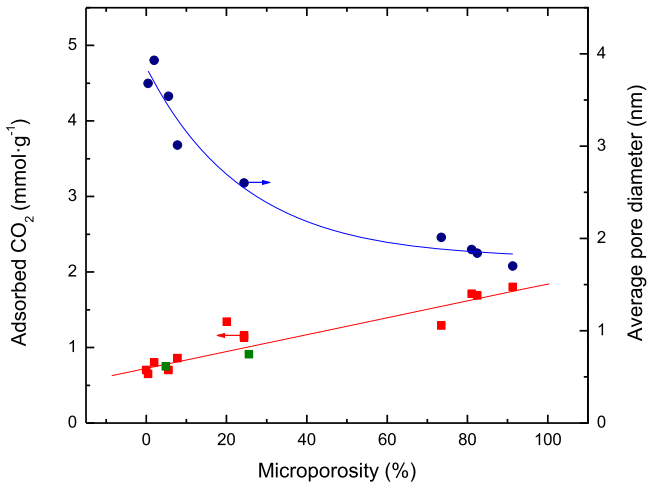

Fig. 7. Effect of microporosity upon adsorption of CO_2 at 15 kPa and average pore size. (¢) [21].

Fig. 7 also shows that the average pore size decreases as microporosity increases. This behavior should be expected, although the pore size distribution can highly influence the average diameter value.

When analyzing the role of the presence of heteroatoms or functional groups in the materials, based on the information provided in Table 1, no clear correlation with CO_2 adsorption values is observed, contrary to what has been observed when analyzing the characteristics of the porous structure of PAN-based carbons (Fig. 7). Therefore, it can be concluded that the role of the porous structure characteristics has a higher weight for evaluating their potential for CO_2 adsorption and separation compared to the influence of the presence of heteroatoms or surface chemistry in these adsorbents.

The experimental CO_2 adsorption data at 0 °C shown in the graphs in Fig. 2 have been fitted using two-parameters widely used models, namely: the Langmuir (eq. (3)), Freundlich (eq. (4)), Temkin (eq. (5)) and Halsey (eq. (6)) isotherms.

$$n = \frac{n_{m,L} \times K_L \times P}{1 + K_L \times P} \tag{3}$$

$$n = K_F \times P^{\frac{1}{n_F}} \tag{4}$$

$$n = B_T \times ln(K_T \cdot P) \tag{5}$$

$$n = \exp\left(\frac{ln(K_H) - ln(P)}{n_H}\right) \tag{6}$$

where n (mmol/g) is the loading of adsorbate, P (kPa) is the pressure and $n_{m,L}$ (mmol·g^{-1}), K_L (1·kPa^{-1}), K_F (mmol·g^{-1}·kPa$^{-1/nF}$), n_F, B_T, K_T (kPa^{-1}), K_H and n_H are isotherms' parameters.

Fig. 8 shows as an example the data fitting to the different models (eqs. (3)-6) for two adsorbents made from PAN. For these adsorbents, it can be observed that Freundlich and Halsey models tend to fit better the experimental data. A similar behavior for Freundlich and Halsey models is observed due to the same linearized equation.

Analyzing the behavior of all the carbons fabricated in the present work, the fitting parameters for the models are shown in Table 4. It also collects the SSR value to assess the model's suitability to the experimental data. It is observed that for all the carbons used for CO_2 adsorption, Freundlich and Halsey models show better behavior than the other models. Temkin model shows the worst behavior, and it is unable to modelize the CO_2 adsorption equilibrium in a satisfactory manner, in agreement with a previous study [42]. Taking into account the non-satisfactory behavior of Temkin isotherm to fit experimental data, this equation has not been used to determine the heat of adsorption

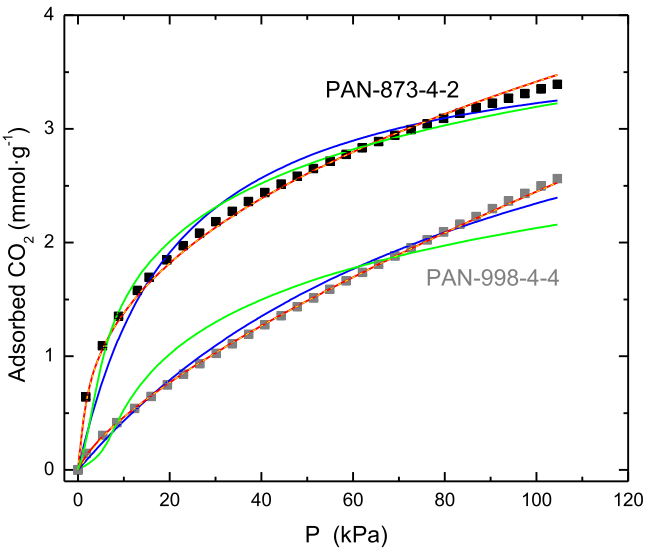

Fig. 8. Experimental data and models for CO_2 adsorption isotherms. (––) Langmuir, (––) Freundlich, (––) Temkin, (––) Halsey isotherms.

for each adsorbent.

Considering the good performance of the Freundlich isotherm for modeling CO_2 adsorption in PAN-based carbons, the fitting parameters shown in Table 4 for this model can be analyzed.

A previous study has concluded that the parameter n_F provides information about the surface characteristics of the material [43]. In this way, it is observed that the n_F parameter reaches higher values for non-activated adsorbents (values between 2.81 and 3.15), indicating that the surface of these materials is more heterogeneous. This conclusion is consistent with a previous study on PAN-derived carbons [21]. For activated carbons, it is observed that the use of low temperature (873 K) allows to reach the highest values of this parameter (ranging from 2.15 to 2.56) because the activation treatment was not very aggressive. When temperatures above 873 K were used, the values of n_F decreased in all cases (ranging from 1.13 to 1.39), which would be related to a more energetically homogeneous surface and support the fact that the adsorption is of a physical type. In all cases, the inverse of n_F takes values between 0 and 1, which allows concluding that the adsorption process is favorable. On the other hand, regarding the value of the K_F parameter, a decrease in its value is observed with increasing the temperature used to fabricate the carbons. Higher values for this parameter indicate stronger interactions between adsorbate and adsorbent.

3.2.1. *Effect of temperature in gas separation process*

Considering both the experimental data previously shown in Fig. 5 and the conclusions reached by other researchers [37], additional work related to gas separation processes by adsorption has been carried out. Specifically, for this part of the work, those carbons that have shown the most interesting characteristics (i.e., high microporosity and surface area based on the data from Table 3) have been selected.

Therefore, studies on CO_2 adsorption at different temperatures have been carried out to obtain more information about the adsorption process in these types of materials. Fig. 9 shows an example of the influence of temperature on the magnitude and shape of CO_2 adsorption isotherms for PAN-1123–0–2. It can be observed that as the temperature, at which the adsorption process occurs, increases, the amount adsorbed decreases significantly. This behavior is consistent with a physical adsorption process. Regarding the shape of the isotherm, no significant changes are observed.

The experimental data for CO_2 adsorption on the selected materials at temperatures different than 273 K have also been fitted using the

Table 4
Adsorption equilibrium parameters of isotherm models for CO_2 at 273 K.

	Langmuir			Freundlich		
Material (PAN-T-S-KOH)	$n_{m,L}$ (mmol·g^{-1})	K_L (kPa^{-1})	SSR	n_F (-)	K_F (mmol·kPa^n·g^{-1})	SSR
PAN–873–2–0	1.21	0.077	0.045	3.15	0.265	0.027
PAN–1123–2–0	2.70	0.062	0.197	2.81	0.482	0.097
PAN–998–4–0	2.15	0.075	0.139	3.12	0.461	0.073
PAN–873–0–2	4.38	0.045	0.574	2.44	0.573	0.060
PAN–1123–0–2	10.28	0.009	0.318	1.29	0.144	0.104
PAN–873–4–2	3.89	0.049	0.491	2.56	0.566	0.055
PAN–1123–4–2	9.29	0.006	0.142	1.20	0.079	0.007
PAN–873–2–4	4.88	0.034	0.626	2.15	0.469	0.028
PAN–1123–2–4	12.02	0.004	0.068	1.13	0.060	0.006
PAN–998–0–4	8.95	0.009	0.409	1.33	0.140	0.001
PAN–998–4–4	4.56	0.070	0.174	1.39	0.089	0.005
PAN–998–2–2	7.67	0.008	0.220	1.29	0.100	0.001
	Temkin			Halsey		
Material (PAN-T-S-KOH)	B_T (-)	K_T (kPa^{-1})	SSR	n_H (-)	K_H (-)	SSR
PAN–873–2–0	0.214	1.58	0.005	−3.15	65.4	0.027
PAN–1123–2–0	0.499	1.08	0.091	−2.81	7.8	0.097
PAN–998–4–0	0.382	1.50	0.023	−3.12	11.2	0.073
PAN–873–0–2	0.835	0.68	0.720	−2.44	3.9	0.060
PAN–1123–0–2	1.418	0.21	7.689	−1.29	12.2	0.059
PAN–873–4–2	0.733	0.78	0.468	−2.56	4.3	0.055
PAN–1123–4–2	1.023	0.19	4.896	−1.20	21.3	0.007
PAN–873–2–4	0.939	0.50	1.383	−2.15	5.1	0.028
PAN–1123–2–4	0.992	0.18	5.245	−1.13	24.3	0.006
PAN–998–0–4	1.252	0.22	6.668	−1.33	13.6	0.000
PAN–998–4–4	0.686	0.22	1.930	−1.39	28.8	0.005
PAN–998–2–2	1.005	0.21	4.509	−1.29	19.3	0.001

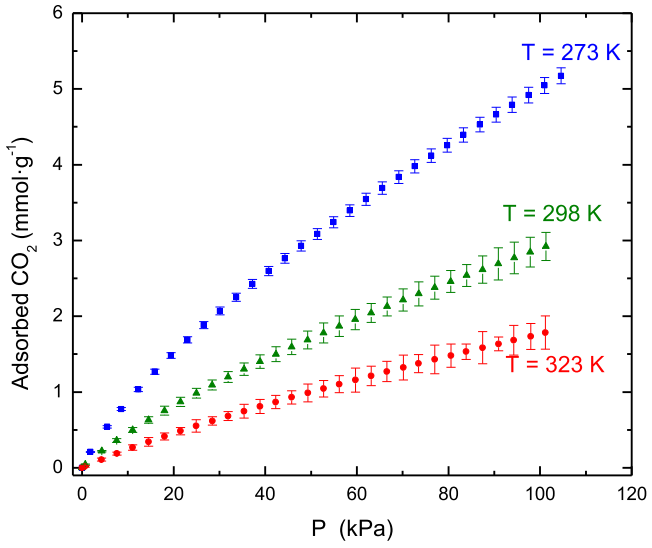

Fig. 9. Influence of temperature upon CO_2 adsorption isotherms using PAN-1123–0–2 carbon.

different models; the corresponding parameters are shown in Tables 5 and 6. It can be observed that, as for CO_2 adsorption at 273 K, the Freundlich model fits the experimental data more satisfactorily at 298 and 323 K. For these temperatures above 273 K, the Langmuir isotherm shows improved performance. In fact, a previous study [42] that analyzed CO_2 adsorption on activated carbons found better performance of the Langmuir isotherm compared to the other models used in the present study. Similarly, it is observed that an increase in temperature tends to decrease the values of the fitting model parameters. The observed decrease in the value of K_F as the temperature increases further confirms the type of physical adsorption previously observed for these materials.

Based on the experimental data regarding the influence of temperature on CO_2 adsorption, the analysis of the heat of adsorption involved can be carried out. This parameter is considered important when evaluating the type of adsorption that occurs and its relation to the adsorbent regeneration stages. This value depends on the interactions between adsorbate and adsorbent and the coverage degree of the adsorbent surface [44], making it important to determine the heat of adsorption in the entire CO_2 adsorption range. For this latter, the Clausius-Clapeyron equation (eq. (7)) has been used.

$$\ln P = \left(\frac{-Q_{st}}{R}\right) \cdot \frac{1}{T} + C \tag{7}$$

where Q_{st} is the isosteric heat of adsorption (kJ mol^{-1}) determined from the slope of the plot of lnP versus 1/T, R is the universal gas constant (8.314 J mol^{-1} K^{-1}), T is the temperature (K), P is the gas pressure, and C is a constant.

The heat of adsorption values determined for the selected carbons are shown in Fig. 10, along with the influence of fabrication conditions and surface coverage degree. First, the magnitude of this parameter was lower than 45 kJ·mol^{-1}, indicating that physical adsorption took place. On the other hand, it can be observed that, generally, there is a decrease in the heat of adsorption as the amount of CO_2 adsorbed increases. This behavior tends to be observed in adsorbents with porosity corresponding to very small pores (i.e., ultramicroporous systems). CO_2 tends to adsorb preferentially in these small pores, where stronger adsorbate-adsorbent interactions occur, which is related to the large heat of adsorption values reached at low surface coverages [45].

Analyzing the influence of fabrication conditions, it can be observed that PAN-1123–0–2 and PAN-998–0–4 show the lowest adsorption heat values. As seen, these materials were produced at higher temperatures, and they also exhibited a lower degree of microporosity. Additionally, high temperatures tend to reduce the functional groups present on the surface of the adsorbent material, affecting the intensity of the adsorbate-adsorbent interactions. The decrease in the intensity of these interactions is consistent with the previous conclusions drawn from the analysis of the fitting parameters of the Freundlich model.

Table 5
Adsorption equilibrium parameters of isotherm models for CO_2 at 298 K.

	Langmuir			Freundlich		
Material	$n_{m,L}$	K_L	SSR	n_F	K_F	SSR
(PAN-T-S-KOH)	(mmol·g^{-1})	(kPa^{-1})		(-)	(mmol·kPa^n·g^{-1})	
PAN–873–0–2	3.10	0.040	0.218	2.43	0.392	0.019
PAN–1123–0–2	7.03	0.007	0.034	1.24	0.072	0.018
PAN–873–4–2	2.82	0.038	0.141	2.38	0.342	0.023
PAN–873–2–4	1.76	0.051	0.047	2.71	0.285	0.031
PAN–998–0–4	5.90	0.007	0.055	1.27	0.069	0.001
	Temkin			Halsey		
Material	B_T	K_T	SSR	n_H	K_H	SSR
(PAN-T-S-KOH)	(-)	(kPa^{-1})		(-)	(-)	
PAN–873–0–2	0.636	0.48	0.192	−2.42	9.7	0.020
PAN–1123–0–2	0.927	0.15	1.404	−1.24	26.1	0.020
PAN–873–4–2	0.595	0.43	0.999	−2.38	12.9	0.024
PAN–873–2–4	0.360	0.62	0.219	−2.70	30.0	0.032
PAN–998–0–4	0.806	0.16	1.192	−1.27	29.9	0.001

Table 6
Adsorption equilibrium parameters of isotherm models for CO_2 at 323 K.

	Langmuir			Freundlich		
Material	$n_{m,L}$	K_L	SSR	n_F	K_F	SSR
(PAN-T-S-KOH)	(mmol·g^{-1})	(kPa^{-1})		(-)	(mmol·kPa^n·g^{-1})	
PAN–873–0–2	2.16	0.040	0.153	1.94	0.178	0.039
PAN–1123–0–2	5.69	0.004	0.007	1.15	0.033	0.009
PAN–873–4–2	2.04	0.031	0.065	1.73	0.122	0.081
PAN–873–2–4	1.37	0.037	0.021	2.09	0.128	0.017
PAN–998–0–4	3.76	0.007	0.033	1.19	0.032	0.001
	Temkin			Halsey		
Material	B_T	K_T	SSR	n_H	K_H	SSR
(PAN-T-S-KOH)	(-)	(kPa^{-1})		(-)	(-)	
PAN–873–0–2	0.490	0.34	0.168	−2.06	27.5	0.012
PAN–1123–0–2	0.664	0.11	0.821	−1.16	50.6	0.005
PAN–873–4–2	0.455	0.29	0.697	−1.91	37.3	0.019
PAN–873–2–4	0.304	0.35	0.236	−2.08	72.2	0.018
PAN–998–0–4	0.504	0.14	0.488	−1.18	58.3	0.001

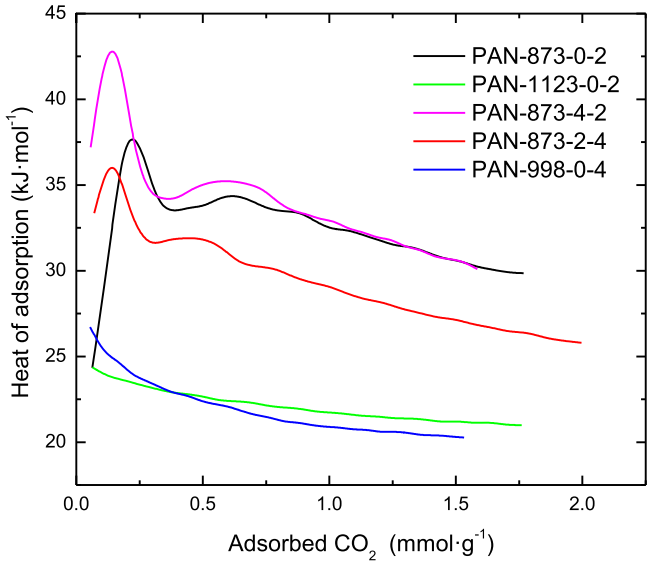

Fig. 10. Influence of adsorbent surface coverage and fabrication conditions upon the heat of adsorption.

The carbons that have shown higher adsorption heat values are fabricated at a temperature of 873 K, with or without the presence of sulfur. The presence of a higher amount of KOH tends to decrease the heat of adsorption, similar to what was observed with the use of higher temperatures. In other words, the more aggressive the activation treatment, the lower is the presence of suitable functional groups in the carbon surface [46].

Using adsorbents for gas separation requires combining a good adsorption capacity with high selectivity toward the gas to be adsorbed in relation to the other gases in the gas stream. For this reason, evaluating the selectivity of the selected materials is necessary. To do this, nitrogen adsorption was performed to assess the behavior of the materials in relation to a typical model stream from a post-combustion process (15 % CO_2 and 85 % N_2). The experiments were carried out using the same experimental procedure as those previously analyzed for CO_2, and Table 7 shows the fitting parameters corresponding to the Langmuir, Freundlich, Temkin and Halsey models.

In contrast to the previously observed behavior for CO_2 adsorption experiments for the different PAN-based carbons, Langmuir, Freundlich and Halsey show suitable behavior to fit adsorption equilibrium experimental data but Langmuir equation reaches the best results. This last model can be considered appropriate for nitrogen due to the non-presence of interactions between adsorbate molecules and the absence of multilayers at the pressure range and temperatures used in these experiments.

To determine the CO_2 selectivity in a binary gas mixture, the IAST (Ideal Adsorbed Solution Theory) model was used, as it considers the competitive adsorption between the gases present in the gas phase in contact with adsorbent material. The data corresponding to the selectivity for the different PAN-based carbons are shown in Fig. 11. It is worth noticing that there are differences among the carbon materials. Particularly, PAN-1123–0–2 and PAN-998–0–4 materials achieve the worst selectivity values regarding CO_2 adsorption in the presence of N_2. These carbons were fabricated using the highest temperatures. This

Table 7
Adsorption equilibrium parameters of isotherm models for N_2 at 273 K.

	Langmuir			Freundlich		
Material	$n_{m,L}$	K_L	SSR	n_F	K_F	SSR
(PAN-T-S-KOH)	(mmol·g^{-1})	(kPa^{-1})		(-)	(mmol·kPa^n·g^{-1})	
PAN–873–0–2	0.61	0.009	$1{\cdot}10^{-4}$	1.20	0.007	0.006
PAN–1123–0–2	2.00	0.004	$2{\cdot}10^{-5}$	1.10	0.009	0.006
PAN–873–4–2	0.89	0.005	$1{\cdot}10^{-6}$	1.13	0.006	0.002
PAN–873–2–4	0.89	0.007	$1{\cdot}10^{-4}$	1.17	0.007	0.012
PAN–998–0–4	2.84	0.002	$2{\cdot}10^{-6}$	1.06	0.007	0.002
	Temkin			Halsey		
Material	B_T	K_T	SSR	n_H	K_H	SSR
(PAN-T-S-KOH)	(-)	(kPa^{-1})		(-)	(-)	
PAN–873–0–2	0.078	0.25	0.018	−1.20	399.0	0.006
PAN–1123–0–2	0.158	0.21	0.115	−1.10	170.1	0.006
PAN–873–4–2	0.083	0.22	0.029	−1.13	352.9	0.002
PAN–873–2–4	0.104	0.24	0.036	−1.17	281.0	0.007
PAN–998–0–4	0.142	0.20	0.111	−1.06	190.6	0.002

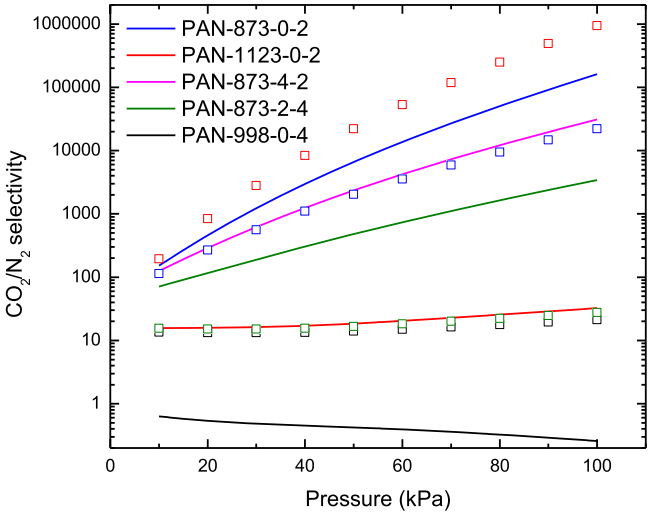

Fig. 11. Influence of fabrication conditions upon CO_2 selectivity for PAN-based carbons [21]: (□) PAN-1073–0–0, (□) PAN-1073–1–0, (□) PAN-1073–0–4, (□) PAN-1073–1–4.

behavior was also observed when the calculated values for the heat of adsorption were analyzed (Fig. 10), where these materials showed the lowest values for this parameter.

In the same way as the heat of adsorption analysis, CO_2 selectivity reaches lower values due to a lower degree of microporosity because the presence of small-sized pores enhances CO_2 adsorption. In fact, regarding the calculated selectivity values, there is a good correlation between the degree of microporosity (see Table 3) and the selectivity values, with an increase in this parameter as microporosity increases.

As previously mentioned, the effect of the presence of heteroatoms was assessed by analyzing the CO_2 loading obtained using the different PAN-based carbons: any type of positive influence on the selectivity values was observed.

Fig. 11 also compares the data obtained for the CO_2 selectivity obtained in the present work with those obtained for PAN-based carbons previously fabricated under different experimental conditions [21]. Some of these carbons reached selectivity values similar to those of the best carbons developed in the present work. The main difference is that, in the previous work, the best carbons were non-activated (PAN-1073–0–0 and PAN-1073–1–0): this means that, despite having high selectivity values, they are not entirely suitable because the adsorption capacity is not very high due to the low surface area achieved as they did not undergo an activation process.

3.3. Application of PAN-carbons in dye adsorption

Based on conclusions from N_2 adsorption isotherms shown in Fig. 4, the materials with lower microporosity and mesoporous do not seem suitable for their use in gas separation processes by adsorption. However, they could be of interest for the separation of larger molecules. The use of adsorption for pollutant removal from aqueous solutions has commonly been focused on dye separation (due to their low concentrations in water). This type of substance usually consists of molecules of high molecular weight and size and is present in the wastewaters of a large number of industries (i.e., textile, wood, etc.). In the present work, a commercial dye (Red GRA 200 %), employed in the wood industry has been selected [22].

The experimental data of dye adsorption capacity and efficiency using the different fabricated materials in the present study are shown in Fig. 12. This figure also indicates the value of the surface area of each of the adsorbent materials to be able to conclude that there is no agreement between this characteristic and the amount of dye adsorbed. For example, the difference between the surface areas of PAN-873–2–4 (with 1115.5 m^2·g^{-1}) and PAN-998–4–4 (with 1701.7 m^2·g^{-1}) would not justify the change observed in the adsorbed amount from 190.2 mg/g (18.2 %) to 1018.2 mg/g (99.8 %).

It can be seen that, under the selected experimental conditions, a very high adsorption occurs using PAN-1123–0–2, PAN-1123–4–2, PAN-1123–2–4, PAN-998–0–4, PAN-998–4–4, and PAN-998–2–2. Based on these results, it can be concluded that the materials classified as mesoporous (except PAN-1123–0–2) achieve a complete removal of this

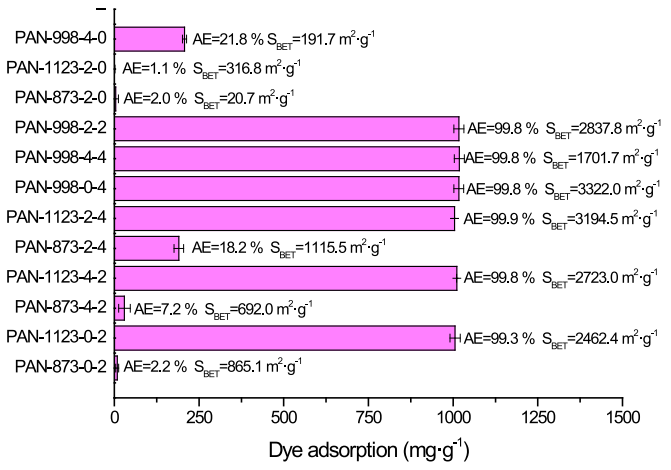

Fig. 12. Dye adsorption capacity and efficiency by PAN-based carbons C_0 = 500 ppm, S/L ratio = 0.5, natural pH (8.02).

pollutant. The difference in the behavior of PAN-1123–0–2 with respect to PAN-873–0–2, PAN-873–4–2, and PAN-873–2–4 in terms of the red dye adsorption may be because, in the case of PAN-1123–0–2, the observed knee (see Fig. 1) is present during a larger relative pressure range, which implies the existence of micropores in a larger size range of this type of pores (i.e. $0.7 < D_p < 2$ nm). These results indicate a certain degree of size exclusion in the most microporous materials since the dependence on the surface area does not show a clear trend.

To confirm this behavior, Fig. 13 shows the influence of the average pore size on the adsorbed amount of dye. It is observed that a pore size of 2 nm or larger allows complete adsorption of the pollutant. Furthermore, it confirms some limitations for the access of molecules into the porous structure or diffusion-type problems. This conclusion agrees with the largest dimension of the dye molecule [22] that has been estimated of around 1.3 nm. For this reason, those carbons with a pore diameter higher than 2 nm have shown an important adsorption capacity since a large part of the pore structure is available for dye adsorption.

Once the role of different operating variables on the structure of the adsorbents, as well as the behavior in CO_2 adsorption and that of GRA-200 %, has been analyzed in detail, Table 8 presents a summary of the observed behaviors. As previously mentioned, it is difficult to draw clear conclusions for some variables, since modifying one operating variable can cause changes in other characteristics of the adsorbents (for example, the effect of temperature on surface area and nitrogen heteroatom content).

Regarding the proposed mechanism by which the adsorption of these two adsorbates preferably occurs on fabricated carbons derived from PAN (Fig. 14), for both molecules (CO_2 and Red dye), the characteristics of the porous structure of the adsorbent appear to play the main role, although in different ways. It should be noted, as previously mentioned, that the greater or lesser presence of heteroatoms, as well as the use of higher or lower temperatures or amounts of activating agent, leads to different characteristics in the porous structure. On one hand, microporosity tends to enhance adsorption at low pressures and selectivity in CO_2 adsorption, due to the fact that the main adsorption mechanism is physisorption—specifically pore-filling (because of the pressure range used) [47]. On the other hand, it generates a size exclusion effect in the case of the red dye. In this latter case, different types of interactions that favor adsorption can occur and are shown in Fig. 14 [48].

Table 9 shows several examples of the behavior of different carbon-based materials, aiming to compare the results obtained in the present study. With regard to CO_2 adsorption, it can be observed that some of the materials made from PAN in this study reach values in the high range

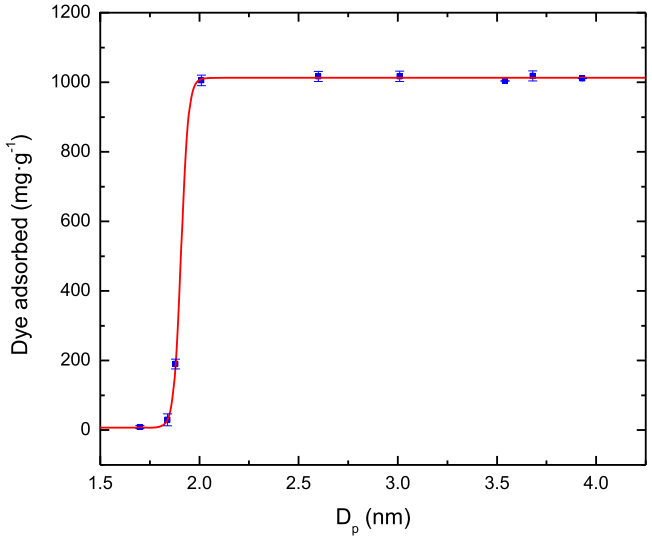

Fig. 13. Effect of average pore diameter upon red dye adsorption capacity. C_0 = 500 ppm, S/L ratio = 0.5, natural pH (8,02).

Table 8
Influence of parameters upon different key characteristics.

	Surface area	Microporosity	CO_2 ads.	Dye ads.
Nitrogen	↘	↗	→	↘
Sulfur	→	↘	↘	→
Potassium hydroxide	↗	→	↗	↗
Temperature	↗	↘	↗	↗

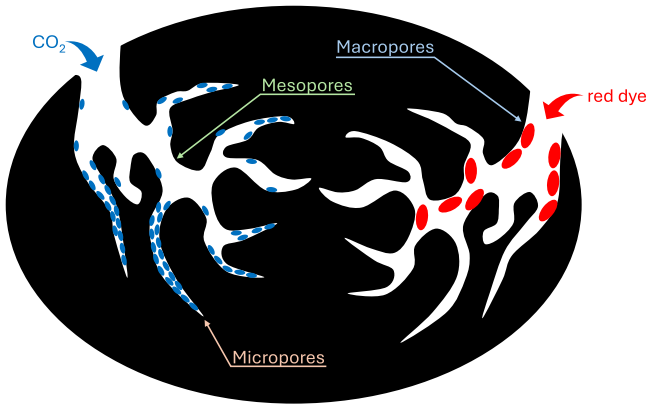

Fig. 14. Diagrammatic representation of pore structure influence upon CO_2 and red dye adsorption.

Table 9
Summary of adsorption capacities for adsorbates used in present work for carbon-based adsorbents.

Adsorbent (precursor)[a]	Adsorbate	Conditions [b] T(K)/t(min)	Uptake (mmol g^{-1})	Ref
OMC (Pluronic F127)	CO_2	C-623/300	3.0	[49]
OMC (N-dopped Pluronic F127)	CO_2	C-673/120 A-1123/120/ KOH	4.9	[50]
GO (N-dopped)	CO_2	C-1073/120	6.5	[51]
CNF (PAN)	CO_2	C-873/180	2.3	[52]
CMF (PAN)	CO_2	C-1173/90	3.4	[53]
AC (PBZC)	CO_2	C-773/60 A-873/60/ KOH	6.7	[54]
Adsorbent (precursor)[a]	Adsorbate	Conditions [b] T(K)/t(min)	Dye uptake (mg g^{-1})	Ref
MWCNT	Acid red 18	purchased	166.7	[55]
MWCNT	Reactive red M-2BE	CCVD	335.7	[56]
Functionalized MWCNT	Congo red	CCVD	148.0	[57]
GO (Graphite)	Direct red 23	C-323/1440	15.3	[58]
GO (Graphite)	Basic red 46	C-323/1440	76.9	[59]
Alkali activated CNF (PAN)	Congo red	C-1173/60	547.6	[60]
Mesoporous CNF (Phenolic resin)	Acid red 1	C-1173/240	493.0	[61]

[a] AC: activated carbon; OMC: Ordered Mesoporous Carbon; GO: Graphene Oxide; CNF: Carbon Nanofibers; CMF: Carbon Microfibers; PBZC: Polybenzoxazine; MWCNT: Multi-walled carbon nanotubes.
[b] Conditions refer to carbon fabrication (C), activation (A), catalytic chemical vapour deposition (CCVD).

(above 5 mmol·g^{-1}) of those shown in Table 9—typically corresponding to activated carbons under conditions similar to those used in this research work. When analyzing the behavior of the adsorbent materials in relation to red dye adsorption, it can be seen that they reach values higher than those reported in the literature, although in these cases the initial concentration of dye in the liquid phase may play a particularly important role.

4. Conclusions

Carbons with different characteristics have been fabricated from PAN using different temperatures and ratios of activating agent (KOH) and doping agent (S) and analysed in relation to the presence of heteroatoms and their porous structure.

The incorporation of sulfur into the carbon structure was demonstrated and enhanced at lower temperatures. This influence was also observed for the presence of nitrogen in the adsorbent materials. The fabrication conditions have significantly influenced PAN-based carbons in relation to their porous structure. The use of higher temperatures and the presence of the activating agent (KOH) tend to increase their specific surface area. However, at the same time, the pore size tends to increase, resulting in mainly mesoporous materials. In contrast, the use of lower temperatures within the studied range and low KOH ratios generates microporous materials, which may show supramicro- or ultramicroporous characteristics. This makes it possible to create tailored carbons for different types of applications.

It has been concluded that characteristics related to the porous structure play a crucial role in CO_2 adsorption, with an enhancement observed in materials with high degree of microporosity, which also showed high selectivity values towards CO_2 in binary mixtures with N_2.

The Freundlich and Halsey models provided the best results when fitting the experimental equilibrium data for CO_2 adsorption at different temperatures, showing that the surface of these carbons is heterogeneous for the gas adsorption. Higher fabrication temperatures tend to generate a more homogeneous surface, and Langmuir model describes better CO_2 adsorption isotherms. In the case of N_2 adsorption, Langmuir, Freundlich and Halsey exhibit a satisfactory behavior.

The importance of the porous structure is also observed in studies with larger molecules (such as a commercial red dye), where a size exclusion phenomenon was observed, completely limiting the dye adsorption in microporous carbons with an average pore size smaller than 2 nm. The strong influence of pore size on dye adsorption makes it difficult to adequately assess other factors such as the presence of heteroatoms or the surface area.

CRediT authorship contribution statement

Lidia Domínguez-Ramos: Validation, Methodology, Investigation. **Diego Gómez-Díaz:** Writing – review & editing, Writing – original draft, Methodology, Investigation. **M. Sonia Freire:** Writing – review & editing, Methodology, Investigation. **Giulio Malucelli:** Writing – review & editing, Investigation. **Massimo Lazzari:** Writing – review & editing, Writing – original draft, Supervision, Project administration, Funding acquisition, Conceptualization. **Julia González-Álvarez:** Writing – review & editing, Supervision, Project administration, Funding acquisition.

Declaration of competing interest

The authors declare that they have no known competing financial interests or personal relationships that could have appeared to influence the work reported in this paper.

Acknowledgements

This work is part of I+D+i project Reference PID2021-122923NB-I00 financed by MCIN/AEI /10.13039/501100011033 / FEDER, UE.

Data availability

The raw/processed data required to reproduce these findings are available upon request.

References

[1] I. Ali, M. Asim, T.A. Khan, Low-cost adsorbents for the removal of organic pollutants from wastewater, J. Env. Manage. 113 (2012) 170–183.
[2] W. Li, B. Mu, Y. Yang, Feasibility of industrial-scale treatment of dye wastewater via bioadsorption technology, Bioresour. Technol. 277 (2019) 157–170.
[3] G. Kyzas, J. Fu, K. Matis, The change from past to future for adsorbent materials in treatment of dyeing wastewaters, Mater 6 (11) (2013) 5131–5158.
[4] L. Pellenz, L.J.S. da Silva, L.P. Mazur, G.M. de Figueiredo, F.H. Borba, A.A. Ulson de Souza, S.M.A. Guelli Ulson de Souza, A. da Silva, Functionalization of graphene with nitrogen-based groups for water purification via adsorption: a review, J. Water Process Eng. 48 (2022) 102873.
[5] T.A. Saleh, Carbon nanotube-incorporated alumina as a support for MoNi catalysts for the efficient hydrodesulfurization of thiophenes, Chem. Eng. J. 404 (2021) 126987.
[6] H.W. Liang, X. Zhuang, S. Brüller, X. Feng, K. Müllen, Hierarchically porous carbons with optimized nitrogen doping as highly active electrocatalysts for oxygen reduction, Nat. Commun. 5 (2014) 4973.
[7] U. Kamran, Y.J. Heo, J.W. Lee, S.J. Park, Chemically modified activated carbon decorated with MnO2 nanocomposites for improving lithium adsorption and recovery from aqueous media, J. Alloys Compd. 794 (2019) 425–434.
[8] H. Zhou, J. Wang, J. Zhuang, Q. Liu, A covalent route for efficient surface modification of ordered mesoporous carbon as high performance microwave absorbers, Nanoscale 5 (2013) 12502–12511.
[9] P. González-García, Activated carbon from lignocellulosics precursors: a review of the synthesis methods, characterization techniques and applications, Renew. Sustain. Energy Rev. 82 (2018) 1393–1414.
[10] Y.J. Heo, Y. Zhang, K.Y. Rhee, S.J. Park, Synthesis of PAN/PVDF nanofiber composites-based carbon adsorbents for CO_2 capture, Compos. B Eng. 156 (2019) 95–99.
[11] M. Zhou, F. Pu, Z. Wang, S. Guan, Nitrogen-doped porous carbons through KOH activation with superior performance in supercapacitors, Carbon. N. Y. 68 (2014) 185–194.
[12] D.J. Babu, M. Bruns, R. Schneider, D. Gerthsen, J.J. Schneider, Understanding the influence of N-doping on the CO_2 adsorption characteristics in carbon nanomaterials, J. Phys. Chem. C 121 (2017) 616–626.
[13] Z. Lin, R. Wang, S. Tan, K. Zhang, Q. Yin, Z. Zhao, P. Gao, Nitrogen-doped hydrochar prepared by biomass and nitrogen-containing wastewater for dye adsorption: effect of nitrogen source in wastewater on the adsorption performance of hydrochar, J. Env. Manag. 334 (2023) 117503.
[14] W. Kiciński, A. Dziura, Heteroatom-doped carbon gels from phenols and heterocyclic aldehydes: sulfur-doped carbon xerogels, Carbon. N. Y. 75 (2014) 56–67.
[15] Y. Shin, G. Fryxell, W. Um, K. Parker, S. Mattigod, R. Skaggs, Sulfur-functionalized mesoporous carbon, Adv. Funct. Mater. 17 (2007) 2897–2901.
[16] D. Saha, G. Orkoulas, J. Chen, D.K. Hensley, Adsorptive separation of CO_2 in sulfur-doped nanoporous carbons: selectivity and breakthrough simulation, Micropor. Mesopor. Mater 241 (2017) 226–237.
[17] J.E. Eichler, J.N. Burrow, N. Katyal, G. Henkelman, C.B. Mullins, Modulation of CO_2 adsorption thermodynamics and selectivity in alkali-carbonate activated n-rich porous carbons, J. Mater. Chem. A 11 (2023) 12811–12826.
[18] K. Sim, N. Lee, J. Kim, E.B. Cho, C. Gunathilake, M. Jaroniec, CO_2 adsorption on amine functionalized periodic mesoporous benzenesilicas, ACS Appl. Mater. Interfaces 7 (2015) 6792–6802.
[19] J. Rivera–Utrilla, I. Bautista–Toledo, M.A. Ferro–García, C. Moreno–Castilla, Activated carbon surface modifications by adsorption of bacteria and their effect on aqueous lead adsorption, J. Chem. Technol. Biotechnol. 76 (2001) 1209–1215.
[20] E. Dautzenberg, S. van Hurne, M.M.J. Smulders, L.C.P.M. de Smet, GraphIAST: a graphical user interface software for ideal adsorption solution theory (IAST) calculations, Comput. Phys. Commun. 280 (2022) 108494.
[21] L. Domínguez-Ramos, A. Prieto-Estalrich, G. Malucelli, D. Gómez-Díaz, M.S. Freire, M. Lazzari, J. González-Álvarez, N- and S-doped carbons derived from polyacrylonitrile for gases separation, Sustainability. 14 (2022) 3760.
[22] C.H. Pimentel, R. Castro-Agra, M.S. Freire, D. Gómez-Díaz, J. González-Álvarez, Adsorption of anionic wood dyes on KOH-activated carbons from Pinus radiata sawdust, Biomass Conv. Bioref. 15 (2025) 7603–7622.
[23] D. Gómez-Díaz, L. Domínguez-Ramos, G. Malucelli, M.S. Freire, J. González-Álvarez, M. Lazzari, S/N/O-enriched carbons from polyacrylonitrile-based block copolymers for selective separation of gas streams, Polymers 16 (2024) 269.
[24] M. Sevilla, A.B. Fuertes, Highly porous S-doped carbons, Micropor. Mesopor. Mater 158 (2012) 318–323.
[25] M. Zhong, E.K. Kim, J.P. McGann, S.E. Chun, J.F. Whitacre, M. Jaroniec, K. Matyjaszewski, T. Kowalewski, Electrochemically active nitrogen-enriched nanocarbons with well-defined morphology synthesized by pyrolysis of self-assembled block copolymer, J. Am. Chem. Soc. 134 (2012) 14846–14857.

[26] I.P. da Paixão Cansado, C.R. Belo, P.A. Mira Mourão, Pesticides abatement using activated carbon produced from a mixture of synthetic polymers by chemical activation with KOH and K_2CO_3, Env. Nanotechnol. Monit. Manag. 12 (2019) 100261.
[27] M. Thommes, K. Kaneko, A. Neimark, J. Olivier, F. Rodriguez-Reinoso, J. Rouquerol, K. Sing, Physisorption of gases, with special reference to the evaluation of surface area and pore size distribution (IUPAC Technical Report), Pure Appl. Chem. 87 (9–10) (2015) 1051–1069.
[28] J.L. Zhang, W.F. Zhang, M.F. Han, J. Pang, Y. Xiang, G.P. Cao, Y.S. Yang, Synthesis of nitrogen-doped polymeric resin-derived porous carbon for high performance supercapacitors, Micropor. Mesopor. Mater 270 (2018) 204–210.
[29] C. Ma, J. Bai, M. Demir, Q. Yu, X. Hu, W. Jiang, L. Wang, Polyacrylonitrile-derived nitrogen enriched porous carbon fiber with high CO_2 capture performance, Sep. Purif. Technol. 303 (2022) 122299.
[30] C. Ma, J. Bai, X. Hu, Z. Jiang, L. Wang, Nitrogen-doped porous carbons from polyacrylonitrile fiber as effective CO_2 adsorbents, J. Env. Sci. 125 (2023) 533–543.
[31] Y. Xu, Z. Yang, G. Zhang, P. Zhao, Excellent CO_2 adsorption performance of nitrogen-doped waste biocarbon prepared with different activators, J. Clean. Prod. 264 (2020) 121645.
[32] J. Serafin, B. Dziejarski, O.J. Fonseca-Bermúdez, L. Giraldo, R. Sierra-Ramírez, M. G. Bonillo, G. Farid, J.C. Moreno-Piraján, Bioorganic activated carbon from cashew nut shells for H_2 adsorption and H_2/CO_2, H_2/CH_4, CO_2/CH_4, $H_2/CO_2/CH_4$ selectivity in industrial applications, Int. J. Hydrog. Energy 86 (2024) 662–676.
[33] J. Shi, N. Yan, H. Cui, Y. Liu, Y. Weng, Sulfur doped microporous carbons for CO_2 adsorption, J. Env. Chem. Eng. 5 (2017) 4605–4611.
[34] Z. Tang, J. Gao, Y. Zhang, Q. Du, D. Feng, H. Dong, Y. Peng, T. Zhang, M. Xie, Ultra-microporous biochar-based carbon adsorbents by a facile chemical activation strategy for high-performance CO_2 adsorption, Fuel Process. Technol. 241 (2023) 107613.
[35] J. Serafin, M. Ouzzine, O.F. Cruz Jr., J. Srénscek-Nazzal, I. Campello-Gómez, F. Z. Azar, C.A. Rey Mafull, D. Hotza, C.R. Rambo, Conversion of fruit waste-derived biomass to highly microporous activated carbon for enhanced CO_2 capture, Waste Manage 136 (2021) 273–282.
[36] J.J. Manyà, B. González, M. Azuara, G. Arner, Ultra-microporous adsorbents prepared from vine shoots-derived biochar with high CO_2 uptake and CO_2/N_2 selectivity, Chem. Eng. J. 345 (2018) 631–669.
[37] E.G. Al-Sakkari, A. Ragab, T.M.Y. So, M. Shokrollahi, H. Dagdougui, P. Navarri, A. Elkamel, M. Amazouz, Machine learning-assisted selection of adsorption-based carbon dioxide capture materials, J. Env. Chem. Eng. 11 (2023) 110732.
[38] C.H. Pimentel, L. Díaz-Fernández, D. Gómez-Díaz, M.S. Freire, J. González-Álvarez, Separation of CO_2 using biochar and KOH and $ZnCl_2$ activated carbons derived from pine sawdust, J. Env. Chem. Eng. 11 (2023) 111378.
[39] V. Rahimi, A. Ferreiro-Salgado, D. Gómez-Díaz, M.S. Freire, J. González-Álvarez, Evaluating the performance of carbon-based adsorbents fabricated from renewable biomass precursors for post-combustion CO_2 capture, Sep. Purif. Technol. 344 (2024) 127110.
[40] W. Cao, H. Xua, X. Zhang, W. Xiang, G. Qi, L. Wan, B. Gao, Novel post-treatment of ultrasound assisting with acid washing enhance lignin-based biochar for CO_2 capture: adsorption performance and mechanism, Chem. Eng. J. 471 (2023) 144523.
[41] L. Xing, F. Yang, X. Zhong, Y. Liu, H. Lu, Z. Guo, G. Lu, J. Yang, A. Yuan, J. Pan, Ultra-microporous cotton fiber-derived activated carbon by a facile one-step chemical activation strategy for efficient CO_2 adsorption, Sep. Purif. Technol. 324 (2023) 124470.
[42] J. Serafin, B. Dziejarski, Application of isotherms models and error functions in activated carbon CO_2 sorption processes, Micropor. Mesopor. Mater 354 (2023) 112513.
[43] M.M. Almoneef, H. Jedli, M. Mbarek, Experimental study of CO_2 adsorption using activated carbon, Mater. Res. Expr. 8 (2021) 065602.
[44] M. Alhassan, M. Auta, J.K. Sabo, M. Umaru, A.S. Kovo, CO_2 capture using amine impregnated activated carbon from Jatropha curcas shell, Br. J. Appl. Sci. Technol. 14 (2016) 1–11.
[45] Y.-C. Chiang, C.-Y. Yeh, C.-H. Weng, Carbon dioxide adsorption on porous and functionalized activated carbon fibers, Appl. Sci. 9 (2019) 1977.
[46] W. Lu, W.M. Verdegaal, J. Yu, P.B. Balbuena, H.K. Jeong, H.C. Zhou, Building multiple adsorption sites in porous polymer networks for carbon capture applications, Energy Env. Sci. 6 (2013) 3559–3564.
[47] C. Xu, W. Wang, K. Wang, A. Zhou, L. Guo, T. Yang, Filling–adsorption mechanism and diffusive transport characteristics of N_2/CO_2 in coal: experiment and molecular simulation, Energy 282 (2023) 128428.
[48] C.H. Pimentel, R. Castro-Agra, M.S. Freire, D. Gómez-Díaz, J. González-Álvarez, Adsorption of anionic wood dyes on KOH-activated carbons from Pinus radiata sawdust, Biomass Conv. Bioref. 15 (2025) 7603–7622.
[49] B. Yuan, X. Wu, Y. Chen, J. Huang, H. Luo, S. Deng, Adsorption of CO_2, CH_4, and N_2 on ordered mesoporous carbon: approach for greenhouse gases capture and biogas upgrading, Env. Sci. Technol. 47 (2013) 5474–5480.
[50] S.M. Mahurin, J. Górka, K.M. Nelson, R.T. Mayes, S. Dai, Enhanced CO_2/N_2 selectivity in amidoxime-modified porous carbon, Carbon. N. Y. 67 (2014) 457–464.
[51] L.P. Guo, Q.T. Hu, P. Zhang, W.C. Li, A.H. Lu, Polyacrylonitrile-derived sponge-like micro/macroporous carbon for selective CO_2 separation, Chem.-Eur. J. 24 (2018) 8369–8374.
[52] V. Selmert, A. Kretzschmar, H. Weinrich, H. Tempel, H. Kungl, R.A. Eichel, CO_2/N_2 separation on highly selective carbon nanofibers investigated by dynamic gas adsorption, ChemSusChem. 15 (2022) e202200761.
[53] R. Ojeda-López, E. Vilarrasa-García, D.C.S. Azevedo, C. Felipe, J.A. Cecilia, E. Rodríguez-Castellón, CO_2 selectivity in CO_2:CH_4 and CO_2:N_2 mixtures on carbon microfibers (CMFs) and carbon microspheres (CMSs), Fuel 324 (2022) 124242.
[54] L. Hong, S. Ju, X. Liu, Q. Zhuang, G. Zhan, X. Yu, Highly selective CO_2 uptake in novel fishnet-like polybenzoxazine-based porous carbon, Energy Fuels. 33 (2019) 11454–11464.
[55] M. Shirmardi, A. Mesdaghinia, A.H. Mahvi, S. Nasseri, R. Nabizadeh, Kinetics and equilibrium studies on adsorption of acid red 18 (Azo-Dye) using multiwall carbon nanotubes (MWCNTs) from aqueous solution, E-J. Chem. 9 (2012) 2371–2383.
[56] F.M. Machado, C.P. Bergmann, T.H.M. Fernandes, E.C. Lima, B. Royer, T. Calvete, S.B. Fagan, Adsorption of reactive Red M-2BE dye from water solutions by multiwalled carbon nanotubes and activated carbon, J. Hazard. Mater. 192 (2011) 1122–1131.
[57] A.K. Mishra, T. Arockiadoss, S. Ramaprabhu, Study of removal of azo dye by functionalized multi walled carbon nanotubes, Chem. Eng. J. 162 (2010) 1026–1034.
[58] W. Konicki, M. Aleksandrzak, D. Moszyński, E. Mijowska, Adsorption of anionic azo-dyes from aqueous solutions onto graphene oxide: equilibrium, kinetic and thermodynamic studies, J. Colloid Interface Sci. 496 (2017) 188–200.
[59] W. Konicki, M. Aleksandrzak, E. Mijowska, Equilibrium, kinetic and thermodynamic studies on adsorption of cationic dyes from aqueous solutions using graphene oxide, Chem. Eng. Res. Des. 123 (2017) 35–49.
[60] B.M. Thamer, A. Aldalbahi, M. Moydeen, A.M. Al-Enizi, H. El-Hamshary, M. Singh, V. Bansal, M.H. El-Newehy, Alkali-activated electrospun carbon nanofibers as an efficient bifunctional adsorbent for cationic and anionic dyes, Colloids Surf. A 582 (2019) 123835.
[61] M. Teng, J. Qiao, F. Li, P.K. Bera, Electrospun mesoporous carbon nanofibers produced from phenolic resin and their use in the adsorption of large dye molecules, Carbon. N. Y. 50 (2012) 2877–2886.